

# Annealing Temperature Effects on the Optical Properties of MnO<sub>2</sub>: Cu Nanostructured Thin Films

S. S. Falahatgar and F. E. Ghodsi\*

Department of Physics, Faculty of Science, University of Guilan, Namjoo Ave., Rasht,  
I. R Iran

(\*) Corresponding author: feghodsi@guilan.ac.ir

(Received: 08 Sept 2013 and Accepted: 18 Jan. 2016)

## Abstract

*In this work, the effect of annealing temperature on the microstructure, morphology, and optical properties of Cu-doped nanostructured MnO<sub>2</sub> thin films were studied. The thin films were prepared by sol-gel spin-coating technique on glass substrates and annealed in the air ambient at 300, 350, 400 and 450 °C temperatures. The structural, morphological and optical properties of the annealed MnO<sub>2</sub>: Cu films have been studied by X-ray diffraction (XRD), Field Emission Scanning Electron Microscopy (FESEM), UV-Vis spectroscopy and Fourier Transform Infrared (FTIR) Spectroscopy. The XRD patterns showed that the crystallinity of the films was decreased with increasing annealing temperature. FE-SEM images of films showed that an increase in annealing temperature affected the densification of the films and increased the porosity of the films. For the first time, the thickness, optical constants and complex dielectric function of MnO<sub>2</sub>: Cu thin films were determined by simulating transmission spectra using Forouhi-Bloomer model in the optimization process. The optical band gap of MnO<sub>2</sub>: Cu thin films were enhanced with increasing annealing temperature from 1.86 eV to 1.98 eV. The presence of Mn-O and other bonds in the films were confirmed by FTIR spectroscopy.*

**Keywords:** Manganese oxide, Doping, Nanostructured thin film, Optical properties, Sol-gel.

## 1. INTRODUCTION

In recent years, preparation of nanostructured materials has attracted much attention due to both scientific interests and potential applications. The nanostructured metal oxides have been widely investigated because of their unique physical and chemical properties compared to bulk materials [1-6]. The metal oxide thin films are an important group of the nanostructured materials. The nano-materials of thin films can be synthesized and grown by different techniques. Thin films can be deposited upon a substrate by different common techniques such as pulsed laser deposition [7], chemical vapour deposition [8, 9] reactive magnetron sputtering [10], spray pyrolysis [11], atomic layer deposition [12], chemical bath deposition [13], sol-gel method [14-16] and so on. Any change in the conditions of the film preparation such as the changes of the deposition technique,

annealing temperature, annealing atmosphere and the presence of additional material (dopant) has a significant effect on the crystalline structure and physical properties. Manganese is a transition metal with variable oxidation states (Mn<sup>+2</sup>, Mn<sup>+3</sup> and Mn<sup>+4</sup>). Shift in oxidation state of manganese is strongly dependent on the conditions of the preparation of manganese oxide material. Manganese dioxide is one of the most attractive inorganic transition metal oxide materials from environmental and economic stand points. It is widely used in biosensors [17], catalysis [18], electrochromic multilayered nano-composite thin films [19, 20], electro-magnetic wave-absorbing layers [21, 22] and high performance electrochemical electrodes and energy storage [23]. The presence of the dopants is an important factor in improving the physical and chemical properties of the products. In

recent years, there has been considerable research efforts focused on the preparation and characterization of doped manganese dioxide thin films. Recently,  $\text{CuBi}_2\text{O}_4$ -doped  $\text{MnO}_2$  electrode has improved the electrochemical performance in  $\text{Na}_2\text{SO}_4$  aqueous solution as electrolyte [24] or Bamboo charcoal (BC)-doped  $\text{MnO}_2$  particles have been suggested as active materials for enhancement of electrochemical performance of capacitors [25]. The compounds such as Al-doped manganese dioxide [26], Ag-doped manganese dioxide [27] and boron doped manganese dioxide [28] were proposed for electrochemical supercapacitors. Some researchers produced nanostructured Cu-doped manganese dioxide layer. In addition to study the electrochemical behavior, they studied the structural, morphology and magnetic characteristics [29-31]. There are a number of studies related to the copper manganese oxide systems. The electronic structure of the  $\text{CuMnO}_2$  was investigated by measuring absorption spectra of the films [32]. In other works, the magnetic properties of  $\text{CuMn}_2\text{O}_4$  [33] and catalytic activity of  $\text{CuMn}_2\text{O}_4$  [34] and  $\text{CuMnO}_2$  [35] were studied. Most studies have been focused on electrochemical properties of thin films, until now; thus, the knowledge of optical properties is quite limited for designing the optical systems. Therefore, determination of optical constants of thin films prepared under various conditions (different atmospheres, pressures, annealing temperatures and dopants) is valuable. In the present work, the nanostructured  $\text{MnO}_2$ : Cu thin films were prepared on glass substrates by sol-gel method under different annealing temperature from 300 to  $450^\circ\text{C}$ . The effect of annealing temperature on the structural, morphological and optical properties of the films has been investigated. The appropriate molar ratio of the copper dopant in the precursor solution was equal to 7%. Since the effects of increasing annealing temperature were investigated,

the concentration of dopant should not be very small. When the concentration of dopant is low, the possibility of the diffusion of all doping impurity into the host lattice is very high and it is expected that the physical properties of the samples do not change significantly with increasing annealing temperature. For the first time, the optical constants and dielectric functions of the nanostructured  $\text{MnO}_2$ : Cu thin films were estimated from the simulated transmission data using Forouhi–Bloomer (FB) dispersion model [36] in an iterative optimization process. The formulation of the FB model is based on the quantum mechanics theory of absorption. Forouhi and Bloomer proposed the explicit expressions for refractive index and extinction coefficient. The optical band gaps and optical constants are derived from the parameters of FB function. The deposition of the films on glass substrates is performed by spin-coating technique due to the low cost and homogeneity of the final products.

## 2. EXPERIMENTAL METHODS

In the sol-gel process, for fabricating the nanostructured  $\text{MnO}_2$ : Cu thin films, the precursor solution was prepared as follows: first, 0.149 g of the copper (II) acetate monohydrate ( $\text{Cu}(\text{CH}_3\text{COO})_2 \cdot \text{H}_2\text{O}$ , Merck) and 2.451 g of the manganese (II) acetate tetra-hydrate ( $\text{Mn}(\text{CH}_3\text{COO})_2 \cdot 4\text{H}_2\text{O}$ , Merck) powders were mixed and dissolved into 25 ml of absolute ethanol ( $\text{C}_2\text{H}_5\text{OH}$ , Merck) solvent and then the precursor solution was stirred with magnetic stirrer at room temperature. The nominal molar ratio of the dopant precursor to the manganese precursor was about 0.07 (or 7 mol %) and the final molarity of manganese precursor in the solution was about 0.4 mol/l. After 5 minutes stirring at room temperature, 0.6 ml of mono-ethanol amine (MEA,  $\text{C}_2\text{H}_7\text{NO}$ , Merck) as the stabilizer was slowly added into the solution. The molar ratio of  $\text{MEA}/\text{Mn}_{(\text{ac})}$  was about 1:1. After stirring for 1.5 hours at room temperature,

the final sol was obtained. The colour of the sol was dark brown, clear and without any suspension of particles. After aging the sol for 24 hours, MnO<sub>2</sub>: Cu layers were deposited onto glass substrates (CAT. NO. 7102) using spin coating technique at 3000 rpm for 10s. Then, the wet films were dried at 150°C in air for 20 min. and heat-treated at temperature range of 300-450°C in ambient air for 1 hour. Since there is the possibility of diffusion of atoms from the substrate into the film, the annealing process was not performed at temperature above 450°C. The produced samples were named as S1, S2, S3 and S4 corresponding to annealing temperature of 300, 350, 400 and 450°C, respectively. X-Ray diffraction (XRD) patterns were obtained using a Philips PW-1800 diffractometer with Cu-K $\alpha$  radiation ( $\lambda=0.15406$  nm). The surface morphology of the films was investigated by the Field Emission Scanning Electron Microscopy (FE-SEM, model Hitachi S-4160). The transmittance of the films in the wavelength range 250–800 nm was measured using a UV–Vis spectrophotometer (Varian Cary 100). The Fourier Transform Infrared transmission spectra (FTIR) were recorded using

Nicolet Magana IR560 Fourier-transformed infrared spectrometer in the range of 3000-475 cm<sup>-1</sup>. The optical properties including optical constants, optical band gap, thickness and dielectric functions of the nanostructured MnO<sub>2</sub>: Cu thin films were calculated by Forouhi-Bloomer model.

### 3. RESULTS AND DISCUSSION

The X-ray diffraction patterns of the nanostructured MnO<sub>2</sub>: Cu thin films (S1, S2, S3 and S4) annealed at temperature range of 300–450°C are shown in Figure 1(a) - (d).

Figure 1(a) (the XRD pattern of S1 annealed at 300°C) shows two peaks at 74.55° and 77.50° corresponding to a (213) oriented Ramsdellite-MnO<sub>2</sub> phase (JCPDS file 44-0142) and an additional phase of Cu<sub>2</sub>O with (222) orientation (JCPDS file 05-0667), respectively.

Recently, Recently, the existence of an additional phase of Cu<sub>2</sub>O in copper doped MnO<sub>2</sub> nanocrystals with 0.1 M of Cu doping have been confirmed by Poonguzhali et al. 29] using X-ray diffraction studies.

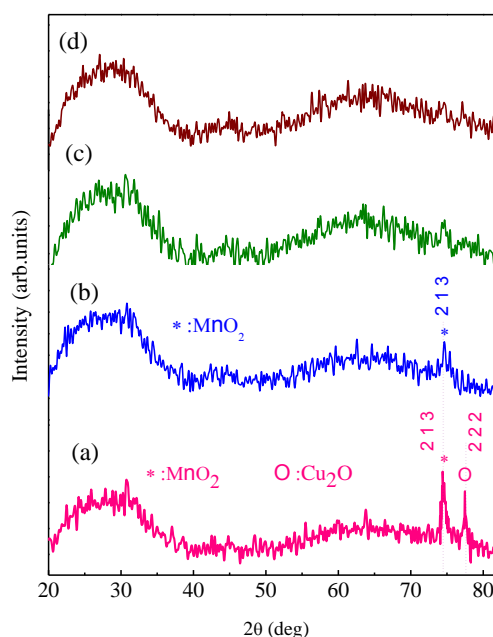


**Figure 1.** XRD patterns of Cu-doped MnO<sub>2</sub> thin films deposited on glass substrates and annealed at various temperatures (a) 300 °C, (b) 350 °C, (c) 400 °C, (d) 450 °C.

They studied X-ray diffraction (XRD) patterns of different levels of Cu doped MnO<sub>2</sub> nanocrystals and observed a small peak of Cu<sub>2</sub>O at higher concentration of Cu dopant. The observed peak at  $2\theta=74.55^\circ$  can be indexed to an orthorhombic MnO<sub>2</sub> phase and corresponding to  $d$ -spacing value ( $d_{hkl}$ ) of 1.27 Å.

The diffraction peak at  $2\theta=77.50^\circ$ , can be indexed to cubic structure of Cu<sub>2</sub>O with  $d_{hkl}$  value of 1.23 Å, lattice constants  $a=b=c=4.26\text{Å}$  and the lattice volume is about  $77.31\text{Å}^3$ . There is a good agreement between obtained  $d$ -values, other calculated parameters from XRD patterns and the standard parameters of JCPDS cards. The lattice parameter of cubic Cu<sub>2</sub>O structure,  $a$ , was calculated by using the formula below [37]:

$$\sin^2(\theta) = \frac{\lambda^2}{4a^2}(h^2 + k^2 + l^2) \quad (1)$$

The average crystallite size ( $D$ ) of sample S1 was estimated using Scherrer's formula [37]:

$$D = \frac{0.9\lambda}{\beta \cos \theta} \quad (2)$$

Where  $D$  is the crystallite size,  $\beta$  is the full width at half maximum (FWHM) intensity of the diffraction peak,  $\lambda$  is the wavelength of the X-ray radiation, and  $\theta$  is the diffraction angle. The average crystallite sizes in the nanostructured thin film S1 (annealed at 300°C) were obtained about 18.5 nm and 27.1 nm for R-MnO<sub>2</sub> (213) and Cu<sub>2</sub>O (222) peaks, respectively. As seen in Figure 1(b), the intensity of the R-MnO<sub>2</sub> (213) X-ray diffraction peak is decreased with increasing annealing temperature. The average crystallite size of the film at 350°C was obtained about 17.5 nm. On the other hand, the second peak corresponding to Cu<sub>2</sub>O (222) disappears with increasing temperature. According to the XRD patterns of Figure 1(c) and (d),

no diffraction peak was observed above the temperature of 350°C caused by the formation of crystalline phases of copper-manganese oxide and other additional phases at higher temperatures. It is attributed to recrystallization and the weak crystallinity nature of the films due to change of annealing temperature. In other words, the appearance of amorphous patterns and the absence of diffraction peaks of Cu<sub>2</sub>O and MnO<sub>2</sub> caused by increasing annealing temperature might be for a number of reasons: (i) the remained Cu impurity appeared as an additional phase at 300°C due to limitation of the incorporation of Cu into MnO<sub>2</sub> crystal structure. When annealing temperature increased, the MnO<sub>2</sub> crystal lattice was reconstructed and the diffusion of Cu ions to MnO<sub>2</sub> lattice enhanced. Then, the crystal structure of S3 and S4 converted to amorphous. (ii) With increasing of annealing temperature, the diffusion of oxygen into the structure of the film increases and Cu<sub>2</sub>O converts to CuO. Hence, CuO becomes more predominant than Cu<sub>2</sub>O at temperatures higher than 350°C [38]. (iii) The MnO<sub>2</sub> phase can be changed to other manganese oxide phases with other oxidation states, because the oxidation state of Mn<sup>+4</sup> decreases at higher temperatures [12].

It is consequently reasonable that the XRD patterns of the sample S3 and S4 can be considered as amorphous oxide material at higher temperatures than 350 °C.

The FE-SEM micrographs of the surface morphologies of Cu-doped MnO<sub>2</sub> nanostructured thin films at four different annealing temperatures are shown in Figure 2(a) - (d). Figure 2(a) shows that the film annealed at 300°C has a granular surface with a uniform distribution of grains and the mean grain dimensions are smaller than 50 nm. Figure 2(b) indicates that the surface morphology has been slightly changed and exhibited a non-uniform distribution of pore within grains for the film annealed at 350°C. With increasing temperature to 400°C, the

micrograph of surface (Figure 2(c)) represents a denser structure with homogeneously distributed fine grains compared to lower temperatures.

At higher temperatures (>400°C), the granular surface morphology is converted to porous amorphous structure which is in agreement with the result of XRD pattern.

The normal transmission spectra of the nanostructured Cu-doped MnO<sub>2</sub> thin films (S1, S2, S3 and S4) deposited on glass substrates were recorded as a function of wavelength ( $\lambda$ ) in the range of 250-800 nm. Figure 3 shows the normal transmission spectra of Cu-doped MnO<sub>2</sub> thin films

The transmittance spectra change with increasing annealing temperature. It can be attributed to the change of thickness of the films and the scattering of incident light from the surface of the films due to the change of the grain size or an increase in the disorder of crystalline structure (see Figure 2).

The optical parameters such as complex refractive index, complex dielectric function, optical band gap and thickness of the films can be obtained from a single transmission spectrum. The geometry model for the prepared samples is considered as air/ (thin) film/ (thick) transparent substrate/air. The complex refractive index  $N(E)$  consists of two parts,  $n(E)$  and  $k(E)$ . The real part,  $n(E)$ , and imaginary part,  $k(E)$ , are usually named refractive index and extinction coefficient, respectively. The theoretical relations that give the measured transmission spectrum as a function of the wavelength ( $\lambda$ ) are defined as below [39].

where  $d_f$  and  $x$  are thickness and the absorbance of thin film, respectively.  $n_s$  is the refractive index of substrate and it is considered a constant value.  $E$  is photon energy.  $h$  is the Planck's constant and  $c$  is the velocity of light. The refractive index,  $n(E)$ , extinction coefficient,  $k(E)$ , and thickness of the Cu-doped MnO<sub>2</sub> films were calculated from the measured transmittance data by Forouhi–Bloomer

(FB) model [36] using Levenberg-Marquardt optimization algorithm [40].

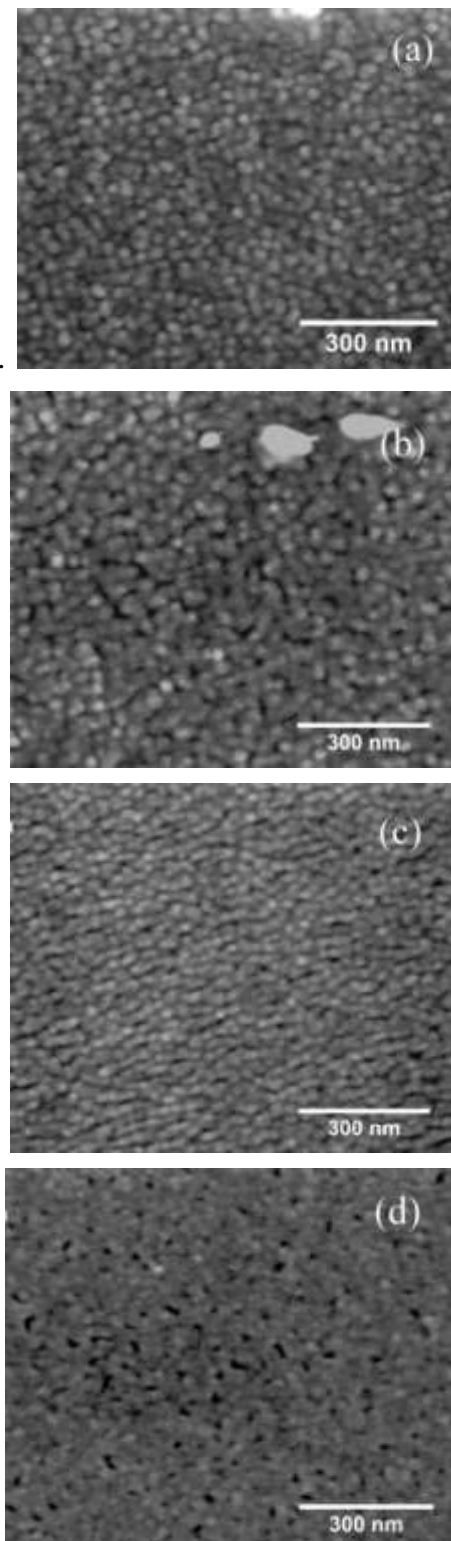


**Figure 2.** The FE-SEM images of Cu-doped MnO<sub>2</sub> thin films annealed at different temperatures (a) 300 °C, (b) 350 °C, (c) 400 °C, (d) 450 °C.

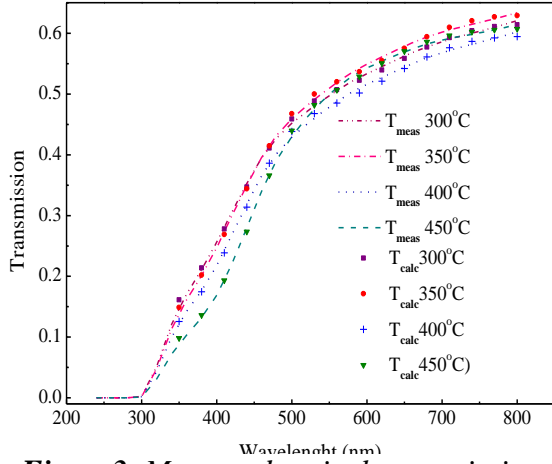


**Figure 3.** Measured optical transmission ( $T_{meas}$ ) and calculated transmission spectra ( $T_{calc}$ ) of Cu-doped  $MnO_2$  thin films annealed at 300, 350, 400 and 450 °C temperatures.

The FB model describes the optical constants of amorphous materials and nano/micro-crystalline system based on quantum mechanical considerations by assuming electronic transitions between the valence and conduction bands.

$$\begin{aligned}
 T &= \frac{Ax}{B - Cx + Dx^2} \\
 A &= 16n_s(n^2 + k^2) \\
 B &= [(n+1)^2 + k^2][(n+1)(n+n_s^2) + k^2] \\
 C &= [(n^2 + k^2 - 1)(n^2 + k^2 - n_s^2) - \\
 &\quad 2k^2(n_s^2 + 1)]2 \cos \varphi \\
 &\quad - k[2(n^2 + k^2 - n_s^2) \\
 &\quad + (n_s^2 + 1)(n^2 + k^2 - 1)]2 \sin \varphi \\
 D &= [(n-1)^2 + k^2][(n-1)(n-n_s^2) + k^2] \\
 \varphi &= \frac{4\pi nd_f}{\lambda}, x = \exp(-\alpha d_f), \quad \lambda = \frac{hc}{E}
 \end{aligned} \tag{3}$$

In this model, both bands are parabolic bands. The dispersion relations of the refractive index,  $n(E)$  and extinction coefficient,  $k(E)$  are given by [36, 41]:

In this model,  $A_i$ ,  $B_i$ , and  $C_i$  depend on the electronic structure and describe the shape of a given peak in the dispersion of

the extinction coefficient.  $E_g$  is the energy band gap of the film.  $n(\infty)$  is the value of the refractive index at infinite photon energy and  $q$  corresponds to the number of peaks in the spectrum of extinction coefficient.

$$\begin{aligned}
 n(E) &= n(\infty) + \sum_{i=1}^q \frac{B_{0i}E + C_{0i}}{E^2 - B_iE + C_i} \\
 k(E) &= \left( \sum_{i=1}^q \frac{A_i}{E^2 - B_iE + C_i} \right) (E - E_g)^2 \\
 B_{0i} &= \frac{A_i}{Q_i} \left( -\frac{B_i^2}{2} + E_g B_i - E_g^2 + C_i \right) \\
 C_{0i} &= \frac{A_i}{Q_i} \left( (E_g^2 + C_i) \frac{B_i^2}{2} - 2E_g C_i \right) \\
 Q_i &= \frac{1}{2} \sqrt{4C_i - B_i^2}
 \end{aligned} \tag{4}$$

The quantities  $B_{0i}$ ,  $C_{0i}$  depend on  $A_i$ ,  $B_i$ , and  $C_i$ . The five parameters of this model i.e.  $A_i$ ,  $B_i$ ,  $C_i$ ,  $E_g$  and  $n(\infty)$  are applied to determine the optical constants of the crystalline and disordered semiconductor. Therefore, the theoretical transmittance spectrum ( $T_{calc}$ ) can be obtained from Equations. (3) and (4). The method in this paper retrieves the optical constants ( $n(E)$ ,  $k(E)$ ) for nanostructured Cu-doped  $MnO_2$  thin films through an iteration process of matching the calculated and measured transmittance spectrum. Therefore, Sum-Square-Error (SSE) is considered as the objective function and is given as:

$$\begin{aligned}
 f(n(\infty), E_g, A_i, B_i, C_i, d_f) &= \\
 \sum_{\lambda} (T_{meas}(\lambda) - T_{calc}(\lambda))^2
 \end{aligned} \tag{5}$$

where  $T_{meas}$  and  $T_{calc}$  indicate the measured and calculated transmittance spectrum, respectively. The optimization process looks for the proper values for fitting parameters that minimize the objective function. Therefore, the calculated transmittance is close to the measured spectrum to full extent. A certain range is defined for each parameter based on a

prior knowledge of the physical properties of the films. A dataset is made of the values of the defined ranges for parameters and considered as input data for the optimization process. The minimization process starts sweeping a thickness range in two stages. First stage determines an initial thickness and best fitting parameters for second stage of minimization with the smaller thickness step size. For confirmation of the applied process, the thicknesses of two samples (S1 and S4) were measured by Stylus profilometer (Dektak) and compared to the calculated thickness values. The calculated thickness values represent differences of about 10, and 15 nm with respect to measured values. The results of the best fitting parameters in Equation (5) and the sum of squared differences between experimental and theoretical transmission data (SSE) are listed in Table 1. The simulated transmission spectra using nonlinear least square fitting procedure are shown in Figure 3.

The refractive index ( $n$ ) and extinction coefficients ( $k$ ) for all samples as a function of the photon energy for different annealing temperatures are shown in Figure 4 (a) and (b). The refractive index (Figure 4(a)) of the nanostructured Cu-doped  $\text{MnO}_2$  thin film decreases with increasing annealing temperature from 300 (S1) to 350°C (S2) and then increases by further increasing of annealing temperature (from 350 (S2) to 400°C (S3)). With increasing temperature to 450°C (S4), the refractive index decreases.

It is attributed to the formation of dense film at 300 °C and 400°C and the increase of porosity and pore size of the films at 350°C and 450°C, which is in agreement with the result of FE-SEM images. The extinction coefficient dispersion (Figure 4(b)) is enhanced with increasing annealing temperature in the energy range of 2.5-3.5 eV, which is related to the change of the crystalline structure of the films and increasing of the scattering from nanograins. The extinction coefficient  $k(E)$

is related to  $\alpha(E)$  as:  $\alpha(E)=4\pi k(E)/\lambda$  [42]. The absorption coefficient can be written as a function of the incident photon energy as below [43]:

$$\alpha E = a(E - E_g)^m \quad (6)$$

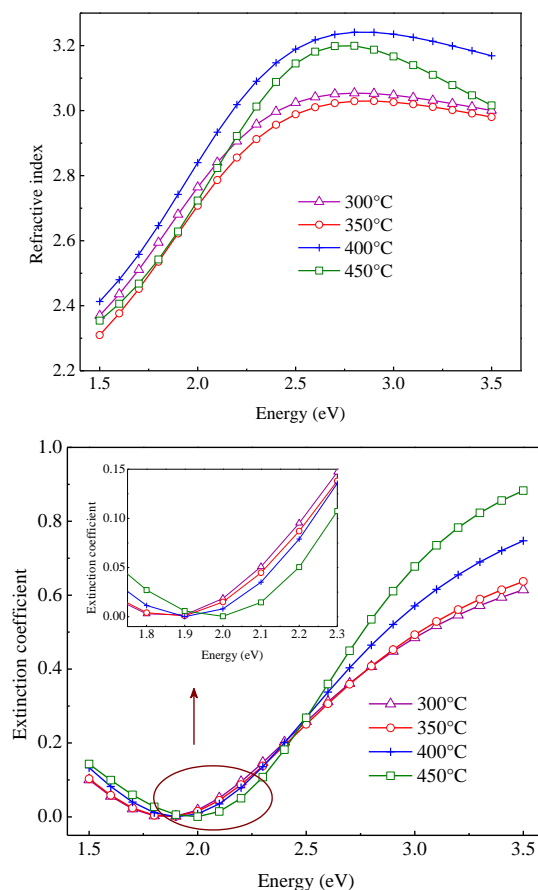


**Figure 4.** (a) Refractive index,  $n$ , and (b) extinction coefficient,  $k$ , of Cu-doped  $\text{MnO}_2$  thin films annealed at 300, 350, 400 and 450 °C temperatures. The inset of figure (b) displays the extinction coefficient in 1.75- 2.3 eV.

where  $a$  is a constant and  $m$  is an exponent that depends on the nature of transitions. The value of  $m$  is 0.5 for direct allowed transition and 2 for indirect allowed transition. The fitting parameters for the optical band gaps i.e.  $E_g$  are listed in Table 1. Equation (6) can be rewritten as:

$$\ln(\alpha E) = \ln(a) + m \ln(E - E_g) \quad (7)$$



The type of transition can be evaluated from Equation (7) by determining the slope of the plot of  $\ln(\alpha E)$  versus  $\ln(E - E_g)$ .

The fitting parameters  $E_g$  or the optical band gaps obtained from FB model were substituted into Equation (7) so that the type of transition can be determined. The type of transitions was the indirect allowed transition with values of  $m$  about 2.

In the Figure 5, the values of slope of the linear fits of  $\ln(\alpha E)$  versus  $\ln(E - E_g)$  confirm the indirect allowed transition for

$\text{MnO}_2$ : Cu thin films. According to Table 1, as the annealing temperature increases from 300 to 450°C, the optical band gaps of the nanostructured  $\text{MnO}_2$ : Cu thin films (S1, S2, S3 and S4) vary from 1.86 to 1.98 eV. From Table 1, it is observed that with increasing annealing temperature, the optical band gap of the films increases and exhibits nearly a 0.12 eV blue shift.

It is related to the reduction in grain size and the change of lattice structure (according to XRD result).

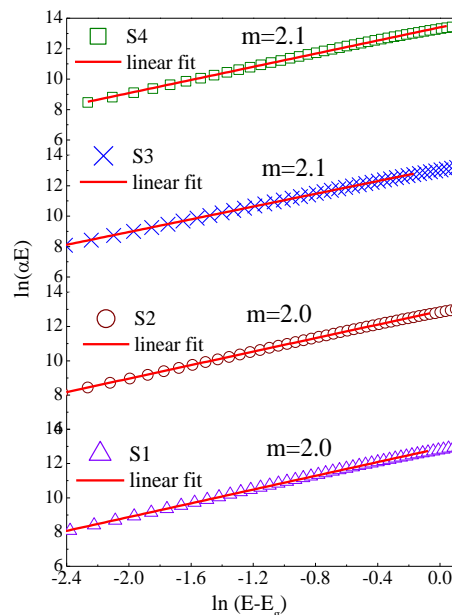


**Figure 5.** The linear fit of  $\ln(\alpha E)$  vs.  $\ln(E - E_g)$  Cu-doped  $\text{MnO}_2$  thin films. The value of  $m$  defines indirect allowed transition.

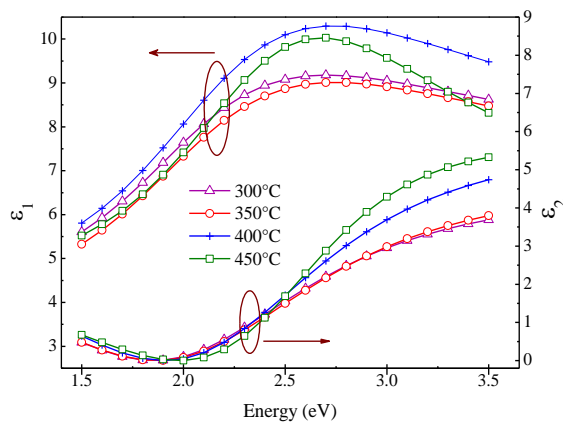


**Figure 6.** Real ( $\epsilon_1$ ) and imaginary ( $\epsilon_2$ ) parts of dielectric function of Cu-doped  $\text{MnO}_2$  thin films annealed at 300, 350, 400 and 450 °C



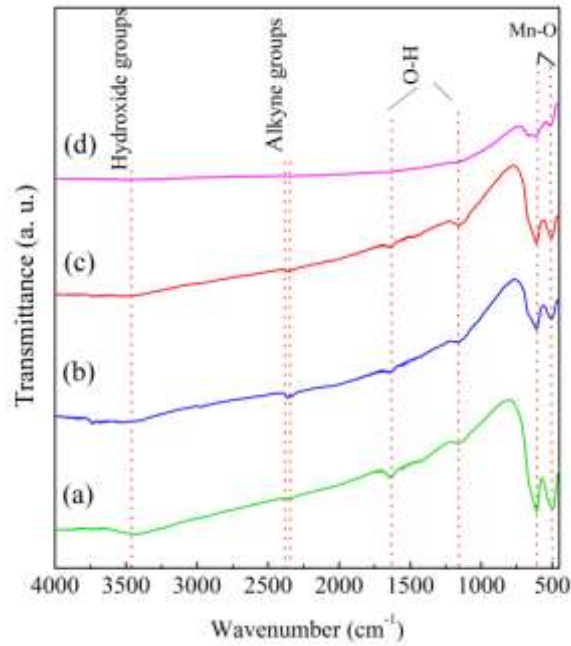


**Figure 7.** The FTIR spectra of Cu-doped  $\text{MnO}_2$  thin films annealed at (a) 300 °C, (b) 350 °C, (c) 400 °C, (d) 450 °C.

**Table 1.** The fitting parameters of FB model for Cu-doped  $\text{MnO}_2$  thin films annealed at various temperatures

Fitting parameters	S1 (300°C)	S2 (350°C)	S3 (400°C)	S4 (450°C)
$E_g$ (eV)	1.86	1.88	1.91	1.98
$A$	0.822	0.896	0.975	0.902
$B$ (eV)	3.70	3.817	3.96	4.55
$C$ (eV)	4.33	4.69	4.92	6.03
$n(\infty)$	2.64	2.58	2.68	2.41
$d_f$ (nm)	64	64	60	60
$SSE$	0.0021	0.0044	0.0049	0.0025

The energy dependent complex dielectric function ( $\varepsilon(E) = \varepsilon_1(E) + i\varepsilon_2(E)$ ) is related to complex refractive index by  $\varepsilon = N^2$ , where  $N(E) = n(E) + ik(E)$ . Therefore,  $\varepsilon_1$  and  $\varepsilon_2$  are related to the real and imaginary parts of the complex refractive index by the following equations [42]:

$$\varepsilon_1 = n^2 + k^2, \varepsilon_2 = 2nk \quad (8)$$

The real and imaginary part of dielectric function for all samples was calculated from Equation (8) and the results are

presented in Figure 6. It is observed that the dispersion of  $\varepsilon_1$  and  $\varepsilon_2$  have very similar behavior to the results of  $n$  and  $k$ . Figure 7 shows the FT-IR spectra of Cu-doped  $\text{MnO}_2$  thin films deposited on glass substrates and annealed at various annealing temperatures. Several absorption bands can be observed in the transmittance spectra about 505, 611, 1157, 1638 and 2370  $\text{cm}^{-1}$ . The absorption peaks around 505 and 611  $\text{cm}^{-1}$  are attributed to the Mn-O vibrations in  $\text{MnO}_6$  octahedral [44-46]. The small absorption peak at around 1157  $\text{cm}^{-1}$  and 1638  $\text{cm}^{-1}$  in the spectrum are the

O–H bending vibrations combined with Mn atoms [44-47]. The minor absorption peak in  $2343\text{ cm}^{-1}$  and  $2370\text{ cm}^{-1}$  may be attributed to alkyne groups [48]. A broad absorption peak at about  $3452\text{ cm}^{-1}$  is associated with the presence of the hydroxide group stretching vibration (-OH group) [47, 48]. From comparison of FTIR spectra of figure 7(a)-(d), it can be inferred that as the temperature is raised from  $300^\circ\text{C}$  to  $450^\circ\text{C}$ , the absorption peaks of organic groups are decreased due to extraction of organic residuals from the thin films.

#### 4. CONCLUSION

The  $\text{MnO}_2$ : Cu thin films were prepared by spin-coating technique on glass substrates at  $300$ ,  $350$ ,  $400$  and  $450^\circ\text{C}$  (S1, S2, S3 and S4) annealing temperature with doping level about 7 mol%. The XRD patterns revealed that the S1 (annealed at  $300^\circ\text{C}$ ) exhibited the orthorhombic phase of  $\text{MnO}_2$  (Ramsdellite) and cubic structure of  $\text{Cu}_2\text{O}$ .

#### REFERENCES

1. Bayansal, F., Kahraman, S., Cankaya, G., Cetinkara, H.A., Guder, H.S., Cakmak, H.M. (2011). "Growth of homogenous CuO nano-structured thin films by a simple solution method," *Journal of Alloys and Compounds* 509: 2094-2098.
2. Hou, Y., Cheng, Y., Hobson, T., Liu, J. (2010). "Design and Synthesis of Hierarchical  $\text{MnO}_2$  Nanospheres/Carbon Nanotubes/Conducting Polymer Ternary Composite for High Performance Electrochemical Electrodes," *Nano Letter* 10: 2727–2733.
3. Yue, G.H., Yan, P.X., Yan, D., Liu, J.Z., Qu, D.M., Yang, Q., Fan, X.Y. (2006). "Synthesis of two-dimensional micron-sized single-crystalline ZnS thin nanosheets and their photoluminescence properties" *Journal of Crystal Growth* 29: 428–432.
4. Ziabari, A. A., Ghodsi, F.E. (2011). "Optoelectronic studies of sol-gel derived nanostructured CdO–ZnO composite films," *Journal of Alloys and Compounds* 509: 8748- 8755.
5. Ji, H., Liu, X., Wang, X. (2010). " $\text{ZrO}_2$ – $\text{SnO}_2$  nanocomposite film containing superlattice ribbons," *Journal of Molecular Structure* 975: 47–52.
6. Dar, M.A., Ahsanulhaq, Q., Kim, Y.S., Sohn, J.M., Kim, W.B., Shin, H.S. (2009). "Versatile synthesis of rectangular shaped nanobat-like CuO nanostructures by hydrothermal method; structural properties and growth mechanism," *Applied Surface Science* 255: 6279–6284.
7. Bea, S. H., Lee, S. Y., Jin, B. J., Im, S. "Growth and characterization of ZnO thin films grown by pulsed laser deposition," *Applied Surface Science* 169 -170: 525-528.
8. Medina-Valtierra, J., Ramirez-Ortiz, J., Arroyo-Rojas, V. M., Ruiz, F. (2003). "Cyclohexane oxidation over  $\text{Cu}_2\text{O}$ – $\text{CuO}$  and  $\text{CuO}$  thin films deposited by CVD process on fiberglass," *Applied Catalysis A* 238: 1-9.
9. Naeem, R., Yahya, R., Pandikumar, A., Huang, N. M., Misran, M., Arifin, Z., Mazhar, M. (2015). "Photoelectrochemical properties of morphology controlled manganese, iron, nickel and copper oxides nanoball thin films deposited by electric field directed aerosol assisted chemical vapor deposition," *Materials Today Communications*4: 141–148.
10. Zhu, H., Zhang, J., Li, C., Pan, F., Wang, T., Huang, B. (2009). " $\text{Cu}_2\text{O}$  thin films deposited by reactive direct current magnetron sputtering," *Thin Solid Films* 517: 5700–5704.

The XRD patterns of the other samples annealed at higher temperatures ( $>300^\circ\text{C}$ ) revealed a decrease in crystallinity and a trend to an amorphous structure. The FE-SEM images showed that the size of nanograins and porosity of surfaces of the films changed as the annealing temperature increased. Hence, the final surface morphology (S4) became porous and amorphous. The refractive index and extinction coefficient dispersion and optical band gap were calculated by Forouhi-Bloomer model using the fitting process of the measured transmission data. The optical band gap of the films increased with increasing the annealing temperature. Formation of Mn-O bond was confirmed from FTIR studies.

#### ACKNOWLEDGEMENT

The authors would like to *acknowledge* the University of Guilan Research Council for the support of this work.

11. Allah, F. K., Abe, S. Y., Nunez, C. M., Khelil, A., Cattin, L., Morsli, M., Bernede, J. C., Bougrine, A., Valle, M. A., Daz, F. R. (2007). "Characterisation of porous doped ZnO thin films deposited by spray pyrolysis technique," *Applied Surface Science* 253: 9241-9247.
12. Nilsen, O., Fjellvag, H., Kjekshus, A. (2003). "Growth of manganese oxide thin films by atomic layer deposition," *Thin Solid Films* 444: 44-51.
13. Unuma, H., Kanehama, T., Yamamoto, K., Watanabe, K., Ogata, T., Sugawara, M. (2003). "Preparation of thin films of MnO<sub>2</sub> and CeO<sub>2</sub> by a modified chemical bath (oxidative-soak-coating) method," *Journal of Materials Science* 38: 255-259.
14. Ching, S., Hughes, S. M., Gray, T. P., Welch, E. J. (2004). "Manganese oxide thin films prepared by nonaqueous sol-gel processing: preferential formation of birnessite," *Microporous and Mesoporous Materials* 76: 41-49.
15. Chen, CY., Wang, SC., Tien, YH., Tsai, WT., Lin, CK. (2009). "Hybrid manganese oxide films for supercapacitor application prepared by sol-gel technique", *Thin Solid Films* 518: 1557-1560.
16. Kim, K. J., Park, Y. R. (2004). "Sol-gel growth and structural and optical investigation of manganese-oxide thin films: structural transformation by Zn doping," *Journal of Crystal Growth* 270: 162-167.
17. Li, L., Du, Z., Liu, S., Hao, Q., Wang, Y., Li, Q., Wang, T. (2010). "A novel nonenzymatic hydrogen peroxide sensor based on MnO<sub>2</sub>/graphene oxide nanocomposite," *Talanta* 82: 1637-1641.
18. Liang, S., Teng, F., Bulgan, G., Zong, R., Zhu, Y. (2008). "Effect of Phase Structure of MnO<sub>2</sub> Nanorod Catalyst on the Activity for CO Oxidation," *Journal of Physical Chemistry C* 112: 5307-5315.
19. Nakayama, M., Kashiwa, Y., Suzuki, K. (2009). "Electrochromic Properties of MnO<sub>2</sub>-Based Layered Polymer Nanocomposite," *Journal of the Electrochemical Society* 156: D125-D130.
20. Sakai, N., Ebina, Y., Takada, K., Sasaki, T. (2005). "Electrochromic Films Composed of MnO<sub>2</sub> Nanosheets with Controlled Optical Density and High Coloration Efficiency," *Journal of the Electrochemical Society* 152: E384-E389.
21. Yuping, D., He, M., Xiaogang, L., Shunhua, L., Zhijiang, J. (2010). "The microwave electromagnetic characteristics of manganese dioxide with different crystallographic structures," *Physica B* 405: 1826-1831.
22. Ting, T.H. (2009). "Effect of Manganese Dioxide Dispersion on the Absorbing Properties of Manganese Dioxide (MnO<sub>2</sub>)-Epoxy Composites," *Journal of the Chinese Chemical Society* 56: 1225-1230.
23. Liu, D., Garcia, B. B., Zhang, Q., Guo, Q., Zhang, Y., Sepelri, S., Cao, G. (2009). "Mesoporous Hydrous Manganese Dioxide Nanowall Arrays with Large Lithium Ion Energy Storage Capacities," *Advanced Functional Materials* 19: 1015-1023.
24. Aref, A.A., Muneerah, A.A., Sun, D.M., Wang, H., Qing, C., Tang, Y.W. (2015). "Preparation and electrochemical capacitance of MnO<sub>2</sub> thin films doped by CuBi<sub>2</sub>O<sub>4</sub>," *Materials Science in Semiconductor Processing* 29: 262-271.
25. Zhang, Y., Yao, Q-q., Gao, H.-li., Zhang, L-sen., Wang, L-z., Zhang, A-q., Song, Y-h., Wang, L-x. (2015). "Synthesis and electrochemical performance of MnO<sub>2</sub>/BC composite as active materials for supercapacitors," *Journal of Analytical and Applied Pyrolysis* 111: 233-237.
26. Li, Y., Xie, H. (2010). "Mechanochemical-synthesized Al-doped manganese dioxides for electrochemical supercapacitors," *Ionics* 16: 21-25.
27. Wang, Y., Zhitomirsky, I. (2011). "Mater. Lett. Cathodic electrodeposition of Ag-doped manganese dioxide films for electrodes of electrochemical supercapacitors," *Materials Letters* 65: 1759-1761.
28. Chi, H. Z., Zhu, H., Gao, L. (2015). "Boron-doped MnO<sub>2</sub>/carbon fiber composite electrode for supercapacitor," *Journal of Alloys and Compounds* 645: 199-205.
29. Poonguzhali, R., Gobi, R., Shanmugam, N., Kumar, A. S., Viruthagiri, G., Kannadasan, N. (2015). "Enhancement in electrochemical behavior of copper doped MnO<sub>2</sub> electrode," *Materials Letters* 157: 116-122.
30. Su, X., Yu, L., Cheng, G., Zhang, H., Sun, M., Zhang, L., Zhang, J. (2014). "Controllable hydrothermal synthesis of Cu-doped δ-MnO<sub>2</sub> films with different morphologies for energy storage and conversion using supercapacitors" *Applied Energy* 134: 439-445.
31. Hashema, A. M., Abuzeid, H. M., Narayanan, N., Ehrenberg, H., Julien, C.M. (2011). "Synthesis, structure, magnetic, electrical and electrochemical properties of Al, Cu and Mg doped MnO<sub>2</sub>," *Materials Chemistry and Physics* 130: 33-38.
32. Hiraga, H., Fukumura, T., Ohtomo, A., Makino, T., Ohkubo, A., Kimura, H., Kawasaki, M. (2009). "Optical and magnetic properties of CuMnO<sub>2</sub> epitaxial thin films with a delafossite derivative Structure," *Applied Physics Letters* 95: 032109-032112.
33. Waskowska, A., Gerward, L., Staun Olsen, J., Steenstrup, S., Talik, E. (2001). "CuMn<sub>2</sub>O<sub>4</sub>: properties and the high-pressure induced Jahn-Teller phase transition," *Journal of Physics: Condensed Matter* 13: 2549-2562.

34. Marban, G., Valdes-Solis, T., Fuertes, A. B. (2007). "High Surface Area  $\text{CuMn}_2\text{O}_4$  Prepared by Silica-Aquagel Confined co-precipitation Characterization and Testing in Steam Reforming of Methanol (SRM)," *Catalysis Letters* 118: 8-14.
35. Rangappa, D., Ohara, S., Umetsu, M., Naka, T., Adschiri, T. (2008). "Synthesis, characterization and organic modification of copper manganese oxide nanocrystals under supercritical water," *Journal of Supercritical Fluids* 44: 441-445.
36. Forouhi, A. R., Bloomer, I. (1988). "Optical properties of crystalline semiconductors and dielectrics," *Physical Review B* 38: 1865-1874.
37. Hammond, C. (2009). *The Basics of Crystallography and Diffraction*, Oxford University Press, New York, pp: 137, 216-219.
38. Pierson, J.F., Thobor-Keck, A., Billard, A. (2003). "Cuprite, paramelaconite and tenorite films deposited by reactive magnetron sputtering," *Applied Surface Science* 210: 359-367.
39. Swanepoel, R. (1983). "Determination of the thickness and optical constants of amorphous silicon," *Journal of Physics E: Scientific Instruments* 16:1214-1222.
40. Sun, W., Yuan, Y. X. (2006). *Optimization Theory and Methods: Nonlinear Programming*, Springer Science, New York, pp. 362-372.
41. Tripura Sundari, S. (2005). "Forouhi-Bloomer analysis to study amorphization in Si," *Journal of Non-Crystalline Solids* 351: 3866-3869.
42. Fujiwara, H.(2007). *Spectroscopic Ellipsometry: Principles and Applications*, John Wiley & Sons, West Sussex UK, pp: 60, 29 and 170.
43. Pankove, J. I. (1971). *Optical Processes in Semiconductors*, New Jersey, Dover, pp: 35-39.
44. Dubal, D.P., Dhawale, D.S., Salunkhe, R.R., Fulari, V.J., Lokhande, C.D. (2010). "Chemical synthesis and characterization of  $\text{Mn}_3\text{O}_4$  thin films for supercapacitor application," *Journal of Alloys and Compounds* 497: 166-170.
45. Julien, C.M., Massot, M., Poinignon, C. (2004). "Lattice vibrations of manganese oxides Part I. Periodic structures," *Spectrochimica Acta Part A: Molecular and Biomolecular Spectroscopy* 60: 689-700.
46. Yousefi, T., Nozad Golikand, A., Mashhadizadeh, M., Aghazadeh, M. (2012). "Template-free synthesis of  $\text{MnO}_2$  nanowires with secondary flower like structure: Characterization and supercapacitor behavior studies," *Current Applied Physics* 12: 193- 198.
47. Dubal, D.P., Dhawale, D.S., Salunkhe, R.R., Pawar, S.M., Lokhande, C.D. (2010). "A novel chemical synthesis and characterization of  $\text{Mn}_3\text{O}_4$  thin films for supercapacitor application," *Applied Surface Science* 256: 4411-4416.
48. Ning, Y.C. (2011). *Interpretation of Organic Spectra*, John Wiley & Sons, Asia, pp: 133-135.